Zero : Jurnal Sains, Matematika, dan Terapan
E-ISSN : 2580-5754; P-ISSN : 2580-569X
Volume 10, Number 2, 2026
DOI: 10.30829/zero.v10i2.28556
Page: 461-473

A Comparison of Generalized Pareto and Weibull Distributions for Modeling Megathrust Seismic Hazard in Indonesia

[1]Aimmatul Ummah Alfajriyah
Department of Actuarial Science, Institut Teknologi Sepuluh Nopember, Surabaya, Indonesia

[2]Moch Taufik Hakiki
Department of Actuarial Science, Institut Teknologi Sepuluh Nopember, Surabaya, Indonesia

[3]Muhammad Haekhal Aqila
Department of Actuarial Science, Institut Teknologi Sepuluh Nopember, Surabaya, Indonesia

Article Info

Article history:

Accepted: 10 July 2026

Keywords:

Extreme Earthquakes;
Generalized Pareto Distribution (GPD);
Parameter Estimation;
Seismic Risk Mapping;
Weibull Distribution.

ABSTRACT

Mapping extreme earthquake risks in Indonesia's megathrust zones is critical for disaster mitigation. This study compares the Generalized Pareto (GPD) and Weibull distributions in modeling extreme earthquake magnitude probabilities. We analyzed 74,514 events (Mw>5.5) across 16 megathrust segments from 1973 to 2024. This data representing a comprehensive large-scale analysis at the national level. To ensure statistical independence of observations, a declustering algorithm was applied to isolate mainshocks. Parameters were estimated using Maximum Likelihood Estimation (MLE) via Nelder-Mead optimization, and evaluated using PDF/CDF plots, AIC, and Cramer-von Mises statistics. Results indicate a significant disparity: the Weibull distribution failed to fit any of the segments, whereas the GPD proved suitable for all 16. Consistently lower AIC and test statistics confirm the GPD's superior accuracy in representing extreme magnitude patterns. Furthermore, return periods and corresponding return levels were calculated to explicitly quantify future extreme seismic hazards.

Corresponding Author:

Moch. Taufik Hakiki
Department of Actuarial Science
Institut Teknologi Sepuluh Nopember
Email: moch.taufik22@its.ac.id

1. INTRODUCTION

Indonesia stands as one of the most seismically vulnerable nations globally, situated at the convergence of three major tectonic plates: the Indo-Australian, Eurasian, and Pacific plates. The potential for earthquakes in the Megathrust zones has re-emerged as a focal point in national disaster mitigation discourse. Specifically, the Meteorology, Climatology, and Geophysics Agency (BMKG) has highlighted the Sunda Strait and Mentawai-Siberut segments as critical zones due to the seismic gap phenomenon, a condition where plate segments remain locked and accumulate energy over extended periods. This accumulation harbors a latent danger of extreme-scale earthquakes, potentially accompanied by tsunamis, necessitating robust mitigation systems [1]. The effectiveness of disaster mitigation strategies relies heavily on the precision of the underlying hazard models. Inaccurate probabilistic assessments, particularly the failure to capture extreme tail distributions, can lead to the underestimation of structural risks and the rapid depletion of post-disaster recovery funds.

In the context of financial mitigation, understanding the physical mechanics of earthquakes is insufficient, precise risk quantification is required for disaster management [2], [3]. Catastrophe Modeling has become crucial for the insurance industry and actuarial institutions to determine premium pricing and risk reserves accurately

[4]. A core component of these models is the Hazard Module, which estimates the probability and intensity of extreme seismic events [4], [5] Inaccuracies in modeling the distribution of extreme magnitudes can lead to significant errors in financial loss estimation, threatening the stability of national disaster funding. Consequently, statistical approaches utilizing Extreme Value Theory (EVT) have become the standard for modeling such tail risks [6], [7], [8], [9], [10]. Existing literature has explored various probability distributions to address these challenges. The Weibull distribution has been validated in several studies for describing general seismic patterns [11], [12], [13], [14], while the Generalized Pareto Distribution (GPD) is often favored for characterizing the tail behavior of extreme data [15]. The application of the Generalized Pareto Distribution (GPD) for modeling seismic data has been extensively addressed in prior studies [16], [17], [18], [19], [20]. Furthermore, parameter estimation via Maximum Likelihood Estimation (MLE), aided by numerical optimization methods, has been widely applied in previous research [21]. However, a significant gap remains in the literature regarding the Indonesian context. Specifically, no comprehensive study has critically compared the performance of GPD and Weibull specifically across Indonesia's 16 Megathrust segments to determine which distribution offers the highest precision for this specific geological domain.

This study presents a framework to quantify extreme seismic risks across 16 megathrust segments in Indonesia. The research is structured around four primary analytical phases. First, a rigorous declustering algorithm is applied to the historical seismic catalog to isolate mainshocks, thereby satisfying the fundamental assumption of statistical independence. Second, parameter estimation is conducted for both the Generalized Pareto Distribution (GPD) and the Weibull distribution using the extreme magnitude data. Third, comprehensive goodness-of-fit evaluations are performed to determine the optimal probability distribution utilizing both visual Goodness-of-Fit indicators and quantitative metrics such as the Akaike Information Criterion (AIC) and the Cramer-von Mises test. Finally, the selected best-fit model is utilized to calculate return periods and their corresponding return levels. Ultimately, this integrated approach provides robust probabilistic baselines to inform national disaster mitigation strategies and resilient infrastructure design.

2. RESEARCH METHOD

2.1 Research Design

This study employs a comparative analysis of the Generalized Pareto Distribution (GPD) and the Weibull distribution to model earthquake moment magnitudes. These distributions, both belonging to the exponential family, were selected due to their established efficacy in extreme risk analysis and tail estimation. Parameters for both distributions are estimated using the Maximum Likelihood Estimation (MLE) method. Given that the probability density functions for GPD and Weibull result in non-closed form solutions, iterative numerical optimization algorithms are employed to derive precise parameter estimates. The statistical adequacy of the fitted models is rigorously evaluated using the Cramer-von Mises statistic. This non-parametric test measures the distance between the empirical distribution function of the observed seismic data and the cumulative distribution function of the models. Models are ranked based on the highest Log-Likelihood values and the lowest Akaike Information Criterion (AIC) scores. This combination is chosen to balance goodness-of-fit with model parsimony, effectively penalizing model complexity to mitigate the risk of overfitting.

2.2 Data Source

This study utilizes secondary data retrieved from the United States Geological Survey (USGS) database. The dataset encompasses seismic events within Indonesia's Megathrust zones with a magnitude of more than 2.5, covering a 50-year period from 1975 to 2024. The key variables analyzed include spatial coordinates, focal depth, and magnitude, as detailed in the Table 1. The "Unit" column specifies the physical measurement standard for each attribute, while "Scale" indicates the level of measurement. All variables are classified as Ratio scale, as they possess a meaningful zero point and allow for the calculation of absolute differences and proportions, which is essential for rigorous Maximum Likelihood Estimation (MLE).

Table 1. Research Variables

Variable	Description	Unit	Scale
Longitude	The longitude coordinate of the earthquake epicenter	Degree	Ratio
Latitude	The latitude coordinate of the earthquake epicenter	Degree	Ratio
Depth	Hypocentral depth below sea level	Km	Ratio
Mw	Earthquake moment magnitude	-	Ratio

The primary standard utilized in modern seismological practice is the moment magnitude (Mw). The moment magnitude is objectively based on the total energy (seismic moment) released by the fault, thus Mw serves as the most consistent measure for seismic hazard analysis. To ensure data homogeneity within a historical earthquake catalog, other magnitude scales are typically converted into Mw equivalents using standard empirical regression equations [4].

Table 2. Earthquake Magnitude Types and Conversion Equations

Magnitude Type	Conversion Equation
M_L	$M_w = M_L$
M_s	$M_w = 0.6016\ M_s + 2.4760$, $2.8 \leq M_s \leq 6.1$ $M_w = 0.9239\ M_s + 0.05671$, $6.2 \leq M_s \leq 8.7$
m_b	$M_w = 1.0107\ m_b + 0.0801$
M_d	$M_w = 0.7170\ M_d + 1.003$

2.3 Earthquake Declustering

In statistical modeling and parameter estimation, the underlying data must strictly satisfy the assumption of being independent and identically distributed (IID). However, in nature, earthquakes do not occur as isolated events but rather as part of a seismic sequence comprising a mainshock, foreshocks, and aftershocks. Foreshocks and aftershocks are triggered by the stress redistribution generated by the mainshock, making their occurrences highly dependent on the primary event. Therefore, prior to probabilistic modeling, a declustering process is mandatory to filter and separate mainshocks (independent data) from dependent earthquakes within the catalog. A widely utilized mathematical algorithm for this purpose is the window method. The window method evaluates a seismic sequence by defining a time window, denoted as $t(M_i)$, and a distance window, denoted as $d(M_i)$, both of which are calculated based on the magnitude of the largest earthquake in a given area (M_i). If an earthquake occurs within the time interval $t(M_i)$ and the spatial radius $d(M_i)$ of a larger event, it is classified as part of the dependent sequence and subsequently eliminated from the mainshock list. In this paper, we use the method proposed by Gardner and Knopoff [4]. In this method, the time window and distance window is given by the Equations (1):

$$t(M_i) = \begin{cases} 10^{0.0320M_i+2.7389} & , M_i \geq 6.5 \\ 10^{0.5409M_i-0.5470} & , M_i < 6.5 \end{cases}, d(Mi) = 10^{0.1238M_i+0.9830} \tag{1}$$

2.4 Generalized Pareto Distribution

The Generalized Pareto Distribution (GPD) is a cornerstone of Extreme Value Theory (EVT), specifically designed to model the tail of a distribution for rare or extreme events. Formally introduced by [22], [23], the GPD is the standard model for exceedances over a high threshold [24]. Consequently, the GPD is a vital tool for risk assessment in environmental studies, finance, and earthquake modeling [25]. The Probability Density Function (PDF) of the GPD is defined as Equation (2):

$$nf(x) = \begin{cases} \frac{1}{\sigma}\left(1 + \frac{\xi(x-\mu)}{\sigma}\right)^{-\frac{1}{\xi}-1} & , \xi \neq 0, \\ \frac{1}{\sigma}\exp\left(-\frac{(x-\mu)}{\sigma}\right) & , \xi = 0. \end{cases} \tag{2}$$

Under the framework of EVT, the GPD is widely employed to model tail data—specifically rare and high severity events such as earthquakes or significant financial losses. The shape parameter ξ is the most important component of the GPD, as it characterizes the tail probability. The value of ξ categorizes the extreme behavior into three distinct domains of attraction, which impacts the physical interpretation of seismic risks [26]. If $\xi > 0$, the distribution is heavy tailed, where the tail of the probability density function decays polynomially. In a seismological context, a positive ξ suggests that the earthquake magnitudes have no theoretical finite upper bound. If $\xi = 0$, the distribution belongs to an exponential distribution, where the tail decays exponentially and thus the distribution is light-tailed. If $\xi < 0$, the distribution falls into Pareto Type II distribution. This domain is characterized by a finite upper bound $x_M = u - \frac{\sigma}{\xi}$. This implies that there is an absolute maximum limit for the extreme seismic event that cannot physically exceeded.

A critical step in GPD application is determining the threshold, which defines the point above which data are considered extreme [25], [26], [27]. Selecting an appropriate threshold is a fundamental. A threshold that is too low may introduce bias into the parameter estimates, whereas a threshold that is too high reduces the number of available observations, thereby increasing variance.

The Mean Residual Life (MRL) plot is a diagnostic tool used to determine the optimal threshold μ for the GPD. This approach is based on the mean excess function, which represents the average of the values exceeding a given threshold. According to [26], the mean excess for a GPD is expressed as Equation (3):

$$e(u) = E[X - u|X > u] = \frac{\sigma + \xi u}{1 - \xi}, \tag{3}$$

where σ is the scale parameter and ξ is the shape parameter. The MRL plot is constructed by plotting the threshold values μ against their corresponding mean excesses. A linear trend in the plot indicates an appropriate threshold range, consistent with the linear property of the mean excess function in a GPD model. This linearity helps distinguish extreme values from the rest of the dataset, ensuring a more accurate model for predicting extreme events. To construct the MRL plot, the data are first ordered from smallest to largest. The plot consists of the following ordered pairs [28] in Equation (4):

$$\left(u, \frac{\sum_{i=1}^{n_u}\left(x_{(i)} - u\right)}{n_u}\right), \tag{4}$$

where n_u represents the number of observations exceeding the threshold u and ξ are the observations that satisfy $x > 0$. The optimal threshold u_0 is selected at the point where the MRL plot exhibits linearity for all higher threshold values.

2.5 Weibull Distribution

The Weibull distribution is a versatile probability distribution that extends the exponential distribution by offering greater flexibility in modeling the hazard function. Unlike the exponential distribution, which is restricted to a constant hazard rate, the Weibull distribution can accommodate increasing or decreasing hazard functions. This adaptability has been empirically proven to make the Weibull distribution suitable for a wide range of variables. Furthermore, it is categorized as one of the three types of extreme value distributions for bounded variables, providing a strong theoretical justification for its application in specific cases. According to [28], the PDF of the Weibull distribution is defined in Equation (5):

$$f(x) = \frac{\beta}{\eta}\left(\frac{x}{\eta}\right)^{\beta-1} \exp\left(-\left(\frac{x}{\eta}\right)^{\beta}\right), \tag{5}$$

where $\beta > 0$ is the shape parameter and $\eta > 0$ is the scale parameter.

2.6 Return Level and Return Period

Let X be a continuous random variable representing the magnitude of an extreme event (e.g., earthquake moment magnitude). The return period, denoted as T, is the expected waiting time (or recurrence interval) between two consecutive events whose magnitudes exceed a specific threshold x. Assuming that the extreme events occur at an average annual rate of λ, based on a Poisson process assumption, the return period (in years) is formulated as shown in Equation (6) [26]:

$$T(x) = \frac{1}{\lambda[1 - F(x)]}. \tag{6}$$

where $F(x)$ is the CDF of X. This metric provides a measure of "how often" an event of intensity x is expected to occur in the long term. The return level, denoted as x_T, is the extreme magnitude (quantile) that is expected to be exceeded, on average, once every T years [26]. The general formulation for the return level is derived using the inverse function of the CDF, that is formulated as Equation (7):

$$x_T = F^{-1}\left(1 - \frac{1}{\lambda T}\right). \tag{7}$$

3. RESULT AND ANALYSIS

3.1 Megathrust Earthquake Data

Data acquisition from the United States Geological Survey (USGS) is subject to specific constraints, notably a maximum limit of 20,000 seismic events per query and the requirement for rectangular geographic bounding boxes. In this paper, we collect the earthquake catalog data on a time frame from 1 January 1975 up until 31 December 2024. We need a large number of data points since we will filter the data in declustering process. The initial dataset presented in Table 2.

Table 2. Number of Seismic Events Before Declustering from 1975 to 2024

Megathrust Segment	Segment Name	Number of Events	Megathrust Segment	Segment Name	Number of Events
M1	Aceh-Andaman	2,543	M9	Jawa Tengah (JT)- Jawa Timur (JTM)	1,026
M2	Nias-Simelue	3,840	M10	Bali	1,064
M3	Batu	164	M11	NTB	621
M4	Mentawai-Siberut	865	M12	NTT	1,278
M5	Mentawai-Pagai	1,908	M13	South Banda Sea	1,996

Megathrust Segment	Segment Name	Number of Events	Megathrust Segment	Segment Name	Number of Events
M6	Enggano	1,318	M14	North Banda Sea	2,390
M7	Sunda Strait (SS)	723	M15	North Sulawesi	769
M8	Jawa Barat (JB)	960	M16	Maluku-Philippine	6,737

Table 2 presents the initial distribution of raw seismic events across the 16 defined Indonesian megathrust segments prior to the declustering process. The data reveals a highly heterogeneous spatial distribution of earthquake frequencies. The Maluku-Philippine segment (M16) exhibits the highest concentration of raw seismic activity with 6,737 recorded events. Both the Nias-Simelue (M2) and Aceh-Andaman (M1) segments also has a massive historical seismicity, which aligns with the highly active subduction dynamics known in the Sumatra trench. The Batu segment (M3) records the lowest number of events: only 164 events. This can be explained by the fact that M3 is geographically a tiny segment compared to other megathrust segment, delineated by highly localized tectonic boundaries

Next, a spatial filtering process was performed using QGIS software to isolate relevant seismic data based on geographic location. The geometric boundaries of the megathrust segments were defined using coordinate points, which were then processed to construct a polygon shapefile representing the specific study zones. This polygon layer served as a spatial mask to filter the comprehensive earthquake catalog, ensuring that only seismic events occurring strictly within the Indonesian Megathrust zones were retained for analysis. The specific geoprocessing workflow executed in QGIS is as follows:

a. Import base map or the administrative boundary shapefile of Indonesia.
b. Import the coordinate points defining the Megathrust segment boundaries.
c. Convert the coordinate points into linear paths using the Points to Path tool.
d. Convert the linear paths into closed areas using the Lines to Polygons tool to define the spatial zones.
e. Data Overlay: Import the complete earthquake dataset (CSV/Spreadsheet) into the map layer.
f. Execute the "Select by Location" algorithm to identify earthquake points that intersect (overlap) with the Megathrust polygons.
g. Export the selected features as a new, filtered dataset for further analysis.

The distinct color coding in the Figure 1 delineates the specific boundaries of the various Megathrust segments.

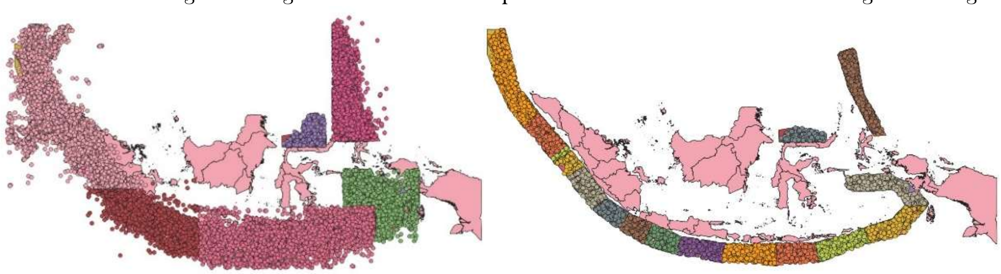

(a) (b)

Figure 1. Selection of Earthquake Data Locations: (a) Data Before Selection; (b) Data After Selection.

3.2 Declustered Data and Its Characteristics

Following the acquisition of the seismic dataset for 16 Megathrust zones, we implement a declustering process to extract the mainshock from the catalog. The main reason for declustering is that the raw earthquake catalogs still consist of a dependent seismic events, namely foreshocks and aftershocks that presents a fundamental statistical challenge. Failing to remove dependent events leads to artificial data clustering, which severely biases the estimation of the parameters, ultimately inflating the calculated probabilities and expected frequencies of extreme mainshocks. This study employed the Gardner-Knopoff declustering algorithm. The final outcome of this procedure is a refined dataset comprising exclusively independent mainshock events, which serves as the definitive baseline for accurate distribution modeling. The number of mainshock from the declustered catalog is given in Table 3.

Table 3. Number of Mainshock by Plate Segmen

Segment	Number of Mainshock	Segment	Number of Mainshock	Segment	Number of Mainshock	Segment	Number of Mainshock
M1	526	M5	303	M9	440	M13	736
M2	319	M6	317	M10	507	M14	714
M3	82	M7	299	M11	379	M15	253
M4	130	M8	328	M12	606	M16	699

3.3 Parameter Estimation

The parameter estimation for GPD is performed using the Maximum Likelihood Estimation (MLE) method. This estimation procedure proceeds under the assumption that the shape parameter $\xi \neq 0$, thereby referring to the PDF equation presented above. Prior to estimating the GPD parameters, the moment magnitude threshold u was determined using the Mean Residual Life (MRL) plot to get a number of candidate thresholds [29]. In this case, that the number of exceedances N_u is at least 30 to ensure that the number of observations are adequate enough. This is to accomadat the segment M3 that has a very small number of mainshock compared to other segments. Subsequently, these candidate thresholds were evaluated through GPD parameter estimation and compared using the Akaike Information Criterion (AIC). The optimal threshold was selected based on the lowest AIC value, subject to the constraint. Suppose that $\mathbf{x} = (x_1, x_2, \ldots, x_n)$ is the observed exceedances of moment magnitude above a threshold that follows GPD. The derivation of the log-likelihood function for the Generalized Pareto Distribution is as follows in Equation (12):

$$\ell(\sigma, \xi|\mathbf{x}) = \ln L(\sigma, \xi|\mathbf{x}) = -n \ln \sigma - \left(\frac{1}{\xi} + 1\right) \sum_{i=1}^{n} \ln\left(1 + \frac{\xi x_i}{\sigma}\right) \tag{12}$$

Differentiating the log-likelihood function in (12) with respect to σ and ξ and equating it to zero, we obtain Equation (13) and (14) successively:

$$\frac{\partial \ell}{\partial \sigma} = 0 \iff -\frac{n}{1+\xi} + \sum_{i=1}^{n} \frac{x_i}{\sigma + \xi x_i} = 0 \tag{13}$$

$$\frac{\partial \ell}{\partial \xi} = 0 \iff \sum_{i=1}^{n} \ln\left(1 + \frac{\xi x_i}{\sigma}\right) - \xi(\xi + 1) \sum_{i=1}^{n} \left(\frac{x_i}{\sigma + x_i \xi}\right) = 0 \tag{14}$$

By solving the simultaneous equations (13) and (14) for σ and ξ we obtain the estimated parameters for GPD. It is evident that the estimators for parameters ξ and σ lack closed-form solutions, thereby requiring numerical iteration. Consequently, GPD parameter estimation is performed computationally using the Nelder-Mead method, which iteratively determines the solutions to the simultaneous equations.

For the maximum likelohood estimators for Weibull distribution, suppose that $\mathbf{x} = (x_1, x_2, \ldots, x_n)$ is the observed moment magnitude from Weibull distribution. The loglikelihood of Weibull distribusion is given by Equation (15):

$$\ell(\beta, \eta|\mathbf{x}) = \log L(\beta, \eta|\mathbf{x}) = n \ln \beta - n\beta \ln \eta + (\beta - 1) \sum_{i=1}^{n} \ln x_i - \frac{1}{\eta^\beta} \sum_{i=1}^{n} {x_i}^\beta \tag{15}$$

Differentiating the log-likelihood function in (15) with respect to σ and ξ and equating it to zero, successively we obtain Equation (16) and Equation (17):

$$\frac{\partial \ell}{\partial \beta} = 0 \iff n\left(\frac{1}{\beta} - \ln \eta\right) + \sum_{i=1}^{n} \ln x_i + \frac{\ln \eta}{\eta^\beta} \sum_{i=1}^{n} {x_i}^\beta - \frac{1}{\eta^\beta} \sum_{i=1}^{n} {x_i}^\beta \ln x_i = 0 \tag{16}$$

$$\frac{\partial \ell}{\partial \eta} = 0 \iff \eta = \left(\frac{\sum_{i=1}^{n} x_i^\beta}{n}\right)^{\frac{1}{\beta}} \tag{17}$$

Based on Equation (17), it is evident that the estimator for parameter η possesses a closed-form solution. However, based on Equation (18), the estimator for parameter β lacks a closed-form solution, thereby requiring numerical iteration.

To quantify the uncertainty or precision of these point estimates, we derive the standard errors using the asymptotic properties of MLE. Asymptotically, the maximum likelihood estimators are normally distributed, where the variance-covariance matrix is the inverse of the expected Fisher information matrix. In practice, this is approximated using the observed Fisher information matrix $\hat{\Sigma}$, which is defined as the negative of the Hessian matrix of loglikelihood ℓ evaluated at the maximum likelihood estimates. For GPD, the standard error estimates for $\hat{\sigma}$ and $\hat{\xi}$ are $SE(\hat{\sigma}) = \sqrt{Var(\hat{\sigma})}$ and $SE(\hat{\xi}) = \sqrt{Var(\hat{\xi})}$ that can be obtained from as shown in Equation (18):

$$\hat{\Sigma} = -H^{-1} = \begin{pmatrix} Var(\hat{\sigma}) & Cov(\hat{\sigma}, \hat{\xi}) \\ Cov(\hat{\xi}, \hat{\sigma}) & Var(\hat{\xi}) \end{pmatrix}, \qquad H = \left.\begin{pmatrix} \dfrac{\partial^2 \ell}{\partial \sigma^2} & \dfrac{\partial^2 \ell}{\partial \sigma \partial \xi} \\ \dfrac{\partial^2 \ell}{\partial \xi \partial \sigma} & \dfrac{\partial^2 \ell}{\partial \xi^2} \end{pmatrix}\right|_{\sigma=\hat{\sigma}, \xi=\hat{\xi}} . \tag{18}$$

where we used $\ell = \ell(\sigma, \xi|\mathbf{x})$ from Equation (12). For Weibull distribution, the standard error estimates for $\hat{\beta}$ and $\hat{\eta}$ can be obtained similarly.

Parameter estimation was performed using numerical methods, specifically, the the Nelder-Mead algorithm. Finally, the model performance was assessed using the Cramér-von Mises goodness-of-fit test. The estimation results are summarized in Table 4. In the estimated value column, the number inside the parnetheses represent the standard error for the parameter estimates.

Table 4. Parameter Estimation and Goodness-of-Fit Test Results for GPD and Weibull Distributions

Megathrust Segment	Parameter Estimated Value	p-Value	Megathrust Segment	Parameter Estimated Value	p-Value
M1	GPD: $u = 5.65$, $\sigma = 0.4491, \xi = -0.0205$	0.075	M9	GPD: $u = 5.45$, $\sigma = 0.3237, \xi = 0.0742$	0.078
	Weibull: $\eta = 5.0250, \beta = 7.9740$	0.000		Weibull: $\eta = 4.9500, \beta = 8.0640$	0.000
M2	GPD: $u = 5.5$, $\sigma = 0.2586, \xi = 0.6669$	0.559	M10	GPD: $u = 5.4$, $\sigma = 0.7484, \xi = -0.6430$	0.120
	Weibull: $\eta = 5.1301, \beta = 5.8269$	0.000		Weibull: $\eta = 4.8782, \beta = 8.2345$	0.000
M3	GPD: $u = 4.7$, $\sigma = 0.5887, \xi = -0.3955$	0.125	M11	GPD: $u = 5.2$, $\sigma = 0.3055, \xi = 0.0570$	0.488
	Weibull: $\eta = 4.9085, \beta = 9.8844$	0.000		Weibull: $\eta = 4.7651, \beta = 8.8416$	0.000
M4	GPD: $u = 5.15$, $\sigma = 0.6788, \xi = -0.1583$	0.4999	M12	GPD: $u = 5.4$, $\sigma = 0.3150, \xi = -0.1557$	0.333
	Weibull: $\eta = 5.1962, \beta = 7.2917$	0.000		Weibull: $\eta = 4.8659, \beta = 10.2346$	0.000
M5	GPD: $u = 5.5$, $\sigma = 0.5875, \xi = 0.1963$	0.284	M13	GPD: $u = 5.55$, $\sigma = 0.4864, \xi = -0.8990$	0.070
	Weibull: $\eta = 5.2558, \beta = 6.3294$	0.000		Weibull: $\eta = 4.9443, \beta = 8.8103$	0.000
M6	GPD: $u = 5.6$, $\sigma = 0.5351, \xi = -0.4719$	0.260	M14	GPD: $u = 5.6$, $\sigma = 0.3454, \xi = 0.0171$	0.133
	Weibull: $\eta = 5.1966, \beta = 9.5298$	0.000		Weibull: $\eta = 4.9818, \beta = 8.9546$	0.000
M7	GPD: $u = 5.5$, $\sigma = 0.4681, \xi = -0.1944$	0.405	M15	GPD: $u = 5.25$, $\sigma = 0.3869, \xi = 0.2745$	0.375
	Weibull: $\eta = 5.1468, \beta = 9.3842$	0.000		Weibull: $\eta = 5.0700, \beta = 7.0360$	0.000
M8	GPD: $u = 5.35$, $\sigma = 0.3850, \xi = 0.0826$	0.339	M16	GPD: $u = 6.05$, $\sigma = 0.7482, \xi = -0.3612$	0.137
	Weibull: $\eta = 5.0378, \beta = 8.0685$	0.000		Weibull: $\eta = 5.2485, \beta = 7.5980$	0.000

Table 4 details the parameter estimates and the Cramer von Mises goodness-of-fit test results for both GPD and Weibull distribution across all 16 Indonesian Megathrust segments. The threshold for extreme magnitudes varies from all segments, ranging from as low as $M_w = 4.7$ in the highly locked Batu segment (M3) to as high as $M_w = 6.05$ in the highly active Maluku-Philippine segment (M16). The goodness-of-fit test results confirming the superiority of the GPD for modeling extreme seismic events on all 16 segemnts. On the other hand, the result for conventional Weibull distribution consistently reject the null hypothesis across all 16 segments.

The estimated shape parameters ξ from the GPD offer a physical insight into the specific tail behavior of each segment. Several segments exhibit positive shape parameters ξ, notably M2 (0.1646), M5 (0.1963), and M15 (0.2745). These positive values suggests that the seismic hazard in these specific zones has a considerable probability for catastrophic earthquake. On the other hand, several other zones, including M3 (-0.3955), M13 (-0.8990), and M16 (-0.3612), yield negative parameter ξ. This behavior indicates a bounded tail and suggests the existence of a finite upper limit to the extreme magnitudes in these areas. Despite the massive frequency of events in M16, its negative shape parameter mathematically implies an absolute physical cap on the maximum tectonic strain release possible within that localized segment geometry.

However, an evaluation of their associated standard errors is important for risk assessment. Several segments, such as M1, M8, and M14, exhibit shape parameters close to zero with a relatively large standard error. Consequently, the 95% confidence intervals for these specific segments includes zero. This implies an inability to reject the null hypothesis of $\xi = 0$, suggesting that the extreme magnitude distributions in these zones might asymptotically approach an exponential tail decay. Thus, we can not confidently rely on a marginally negative point estimate, since the upper confidence limits of these segments extend into the positive domain. The potential for heavy-tailed, theoretically unbounded catastrophic events, cannot be ruled out. Therefore, the formulation of disaster mitigation policies in these segments, must incorporate the upper bounds of the parameter confidence intervals to prevent the severe underestimation of long-term return levels.

3.4 Probability Density Plot

Following the acquisition of parameter estimates for the two distributions, the analysis proceeds with the visualization of probability density plots. The resulting plots, comparing the earthquake data with the estimated parameters, are presented below. The GPD demonstrates superior performance, particularly in capturing the tail behavior of the dataset. This capability aligns with the fundamental characteristics of the Generalized Pareto Distribution in modeling extreme values for risk analysis. In contrast, the Weibull distribution shows limitations in capturing the complex variability of the M_w data. This is indicated by a significant lack of fit in both the center and the tail of the distribution, resulting in the model's failure to accurately represent the empirical data patterns. The visual evaluation of the model fit is presented in Figure 2. In this PDF plot, the x-axis denotes the earthquake moment magnitude M_w, while the y-axis represents the corresponding probability density.

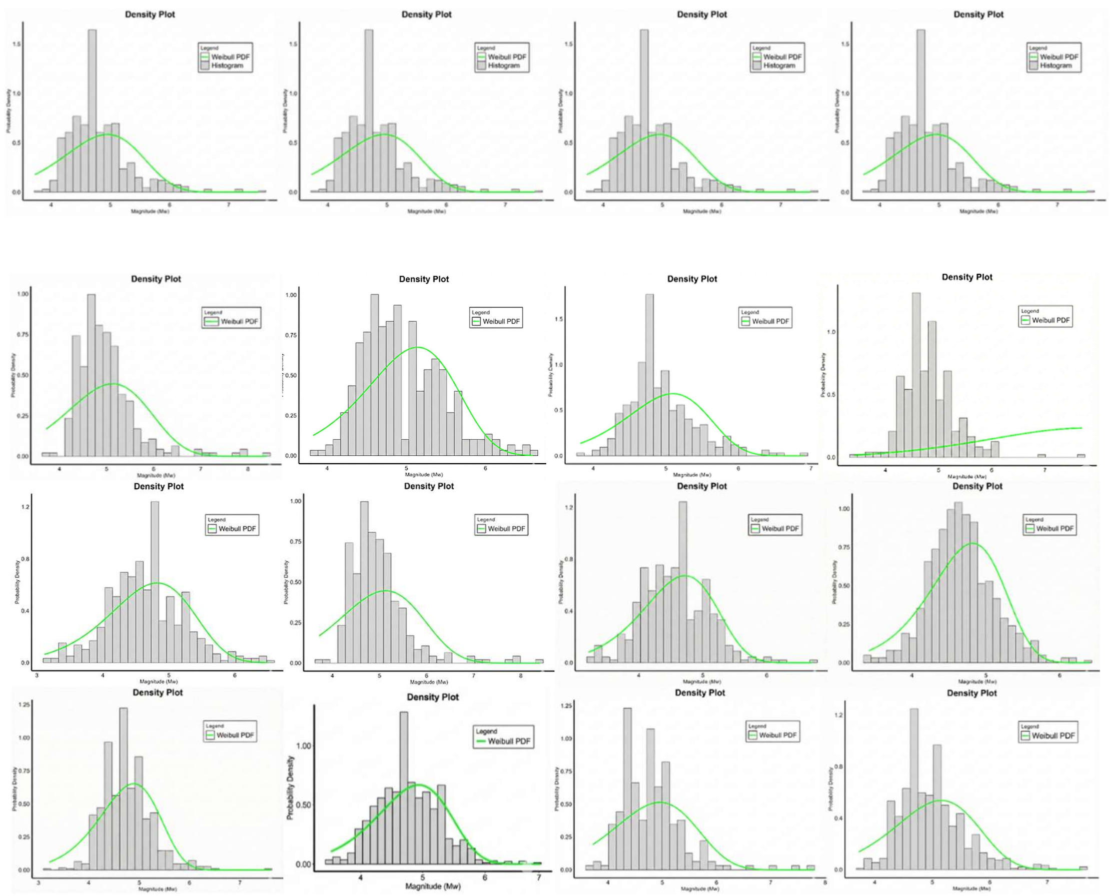

Figure 2. Probability Density Function (PDF) Plots of the Generalized Pareto Distribution (GPD) for 16 Megathrust Segments.

Figure 3 illustrating the goodness-of-fit for the Weibull distributions. The x-axis represents the earthquake moment magnitude M_w and the y-axis represents the probability density, showing how each model fits the observed extreme seismic data. The vertical dashed line marks the threshold of $M_w = 5.5$. As visually evident against the empirical data histogram, the GPD provides a superior fit for the extreme magnitudes, whereas the Weibull distribution fails to adequately represent the original data distribution above the threshold.

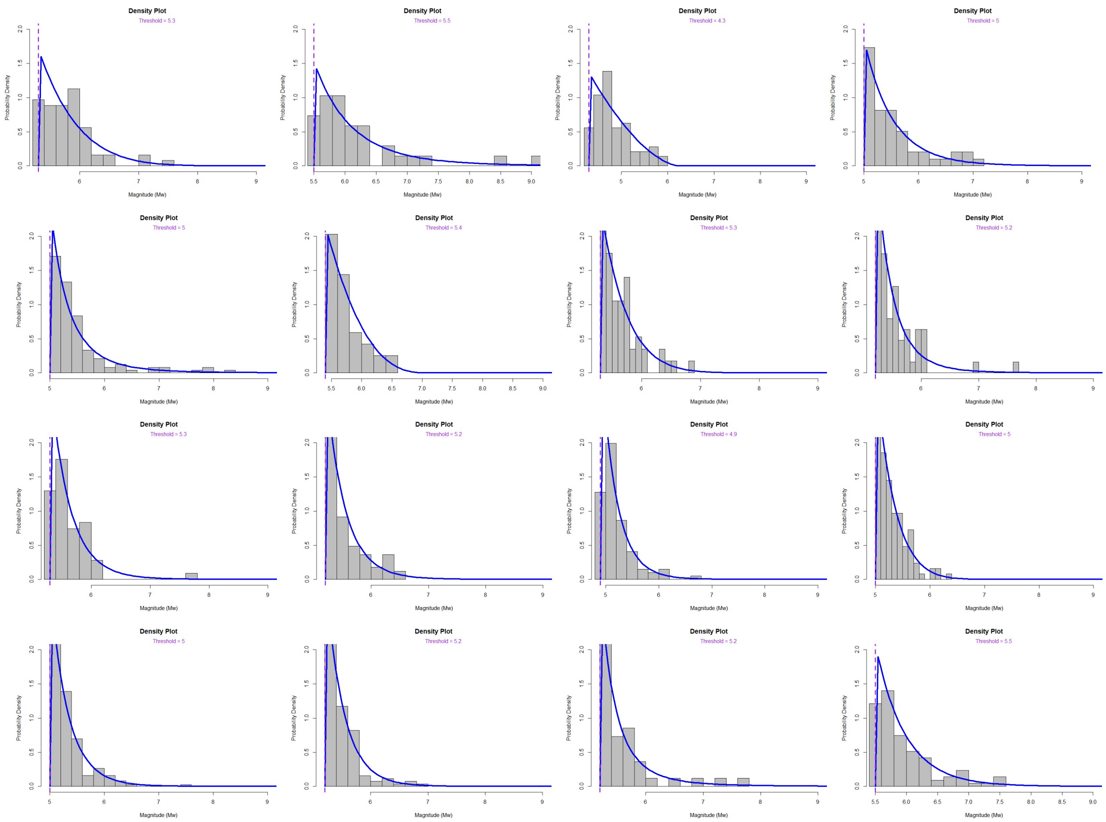

Figure 3. Probability Density Function (PDF) Plots of the Weibull Distribution for 16 Megathrust Segments

3.5 Return Period and Return Level

Using Equation (6) and (7), we can now calculate the yearly return period and return level on all 16 mega thrust segment, where the occurrence rate parameter λ represents the average number of earthquakes with magnitudes exceeding the threshold u within a one-year period. We use the GPD as the base distribution, since it is the best fit for each segment. The result for return period and return level are summarized in Table 5. As an important note, the calculation of the recurrence interval for each segment is intentionally truncated at the first magnitude value that yields an estimated time exceeding 1,000 years. This truncation is performed because beyond that point, the return period values would surge to absurdly high levels As for the calculation of return level, we focus on time period up to 1,000-year horizon. However, evaluations for several segments were deliberately truncated before reaching 1,000 years if the projected return level exceeded 10.0 Mw. Physically, the Earth's faults lack the physical dimensions required to accommodate ruptures beyond this scale.

Table 5. Return Period of the Moment Magnitude for Its Corresponding Magnitude and Return Level of the Moment Magnitude for Corresponding Recurrent Period

Segment	Occurrence Rate, λ	Threshold, u	Theoretical Max, Mwmax	Magnitude (Return Period in Years)	Period in years (Return Level Mw)
M5	0.64	5.15	-	6.0 (3), 6.5 (6), 7.0 (11), 7.5 (19), 8.0 (31), 8.5 (49), 9.0 (74)	50 (8.52), 100 (9.40)
M6	0.64	5.60	6.72	6.0 (4), 6.5 (43)	50 (6.52), 100 (6.57), 200 (6.62), 500 (6.65), 1000 (6.67)
M7	0.62	5.50	7.91	6.0 (5), 6.5 (25), 7.0 (244)	50 (6.67), 100 (6.83), 200 (6.96), 500 (7.12), 1000 (7.22)

Segment	Occurrence Rate, λ	Threshold, u	Theoretical Max, Mwmax	Magnitude (Return Period in Years)	Period in years (Return Level Mw)
M8	0.72	5.35	-	6.0 (7), 6.5 (20), 7.0 (54), 7.5 (137), 8.0 (323), 8.5 (729), 9.0 (1526)	50 (6.96), 100 (7.32), 200 (7.72), 500 (8.27), 1000 (8.71)
M9	0.68	5.45	-	6.0 (7), 6.5 (27), 7.0 (89), 7.5 (264), 8.0 (727), 8.5 (1863)	50 (6.75), 100 (7.05), 200 (7.37), 500 (7.81), 1000 (8.17)
M10	0.72	5.40	6.54	6.0 (4), 6.5 (173)	50 (6.45), 100 (6.48), 200 (6.50), 500 (6.52), 1000 (6.53)
M11	0.60	5.20	-	6.0 (4), 6.5 (19), 7.0 (75), 7.5 (268), 8.0 (2655)	50 (6.35), 100 (6.61), 200 (6.88), 500 (7.26), 1000 (7.56)
M12	0.70	5.40	7.42	6.0 (14), 6.5 (220), 7.0 (32925)	50 (6.26), 100 (6.38), 200 (6.49), 500 (6.61), 1000 (6.69)
M13	0.60	5.55	10.5	6.0 (4), 6.5 (15), 7.0 (57), 7.5 (275), 8.0 (1778)	50 (6.95), 100 (7.19), 200 (7.40), 500 (7.67), 1000 (7.86)
M14	0.68	5.60	-	6.0 (5), 6.5 (19), 7.0 (74), 7.5 (282), 8.0 (1043)	50 (6.86), 100 (7.11), 200 (7.37), 500 (7.72), 1000 (7.98)
M15	0.72	5.25	-	6.0 (7), 6.5 (14), 7.0 (26), 7.5 (45), 8.0 (72), 8.5 (108), 9.0 (157)	50 (7.61), 100 (8.40), 200 (9.36)
M16	0.66	6.05	8.12	6.5 (3), 7.0 (8), 7.5 (42), 8.0 (3893)	50 (7.54), 100 (7.67), 200 (7.77), 500 (7.87), 1000 (7.92)

Table 5 presents the return periods for large and moment magnitudes. Segments with a positive shape parameter ξ lack a theoretical maximum magnitude. Our model estimates that the return period for earthquake event with 9.0 Mw is more than 1000 years, which strongly correlates to historical extreme earthquakes, notably the 2004 Aceh (9.1-9.3 Mw) in M1. The relatively short return periods for extreme magnitudes in these zones highlight an urgent need for earthquake-resistant infrastructure. Conversely, segments with a negative shape parameter ξ, such as M3, M10, and M12 exhibit a theoretical physical limit to seismic energy. Table 5 also presents the estimated return levels of moment magnitude for time horizons from 50 years to 1000 years. In segments with a positive shape parameter ξ, such as M2, M5, and M15, return levels escalate beyond extreme magnitude of 10.0 Mw over longer time horizons. In practical terms, an earthquake with 8.5 Mw or larger in these segments would trigger shaking intensities with MMI (Modified Mercalli Intensity) scale around IX to XI (violent to extreme) in coastal areas, potentially generating catastrophic tsunamis and city-wide structural collapses. Conversely, in segments with a theoretical maximum bound, the return level flattens rapidly and will never intersect or exceed this upper limit. This characteristic is evident in segments M3 and M10.

4. CONCLUSION

This study presents a robust probabilistic evaluation of extreme seismic hazards across 16 megathrust segments in Indonesia. By strictly isolating statistically independent mainshocks through a declustering process, the comparative analysis yielded unequivocal results regarding the performance of the GPD and Weibull distributions. Empirical evaluations, supported by visual diagnostics, AIC, and Cramer-von Mises statistics, demonstrated a significant performance disparity. The GPD exhibited superior accuracy, successfully capturing the heavy-tailed of extreme earthquake magnitudes and providing a statistically fit for all 16 analyzed segments. In contrast, the Weibull distribution proved structurally inadequate. Furthermore, the optimal GPD model was utilized to calculate segment-specific return periods and corresponding return levels for a 1,000-year timeframe. These probabilistic metrics explicitly quantify future megathrust earthquake risks. A limitation of this study lies in the declustering process; the reliance on conventional methods for mainshock identification has the inherent drawback of eliminating the dependency structures between seismic events.

ACKNOWLEDGEMENT

This work was supported by the Institut Teknologi Sepuluh Nopember (ITS) under research grant No. 2747/PKS/ITS/2025. The authors gratefully acknowledge all contributors for their support during the completion of this study.

5. REFERENCES

[1] S. Pasari, A. V. H. Simanjuntak, A. Mehta, Neha, and Y. Sharma, “The Current State of Earthquake Potential on Java Island, Indonesia,” *Pure Appl. Geophys.*, vol. 178, no. 8, pp. 2789–2806, Aug. 2021, doi: 10.1007/s00024-021-02781-4.

[2] M. Foote, J. Hillier, K. Mitchell-Wallace, and M. Jones, *Natural catastrophe risk management and modelling*. Wiley, 2017. doi: 10.1002/9781118906057.

[3] C. A. Isnard and E. C. Zeeman, “Some models from catastrophe theory in the social sciences,” in *The Use of Models in the Social Sciences*, vol. 1, L. Collins, Ed., Routledge, 1976, pp. 38–75. doi: 10.4324/9781315014227.

[4] D. R. Tampubolon, R. Pratama, and A. Y. Gunawan, “Modeling the risk of financial losses due to tectonic earthquakes: Case study on damages to school buildings in a region in Indonesia,” 2024, p. 060001. doi: 10.1063/5.0171170.

[5] P. Taylor, “Calculating Financial Loss from Catastrophes,” in *Earthquake Risk and Engineering towards a Resilient World*, Cambridge: SECED, Jul. 2015, pp. 1–15.

[6] M. I. Gomes and A. Guillou, “Extreme Value Theory and Statistics of Univariate Extremes: A Review,” *International Statistical Review*, vol. 83, no. 2, pp. 263–292, Aug. 2015, doi: 10.1111/insr.12058.

[7] W. Anggraeni, S. Supian, Sukono, and N. B. A. Halim, “Earthquake Catastrophe Bond Pricing Using Extreme Value Theory: A Mini-Review Approach,” *Mathematics*, vol. 10, no. 22, p. 4196, Nov. 2022, doi: 10.3390/math10224196.

[8] J. Beirlant, A. Kijko, T. Reynkens, and J. H. J. Einmahl, “Estimating the maximum possible earthquake magnitude using extreme value methodology: the Groningen case,” *Natural Hazards*, vol. 98, no. 3, pp. 1091–1113, Sep. 2019, doi: 10.1007/s11069-017-3162-2.

[9] R. Shcherbakov, J. Zhuang, G. Zöller, and Y. Ogata, “Forecasting the magnitude of the largest expected earthquake,” *Nat. Commun.*, vol. 10, no. 1, p. 4051, Sep. 2019, doi: 10.1038/s41467-019-11958-4.

[10] C. T. Guloksuz and N. Celik, “An Extension of Generalized Extreme Value Distribution: Uniform-GEV Distribution and Its Application to Earthquake Data,” 2020. [Online]. Available: http//:statassoc.or.th

[11] M.-H. Wu, J. P. Wang, and K.-W. Ku, “Earthquake, Poisson and Weibull distributions,” *Physica A: Statistical Mechanics and its Applications*, vol. 526, p. 121001, Jul. 2019, doi: 10.1016/j.physa.2019.04.237.

[12] A. Arshad, A. H. Hasan, and S. M. Ahmed, “Optimizing Weibull Distribution Parameters for Improved Earthquake Modeling in Japan: A Comparative Approach,” *International Journal of Neutrosophic Science*, vol. 24, no. 1, pp. 65–73, 2024, doi: 10.54216/IJNS.240106.

[13] K. H. Coban and N. Sayil, “Evaluation of earthquake recurrences with different distribution models in western Anatolia,” *J. Seismol.*, vol. 23, no. 6, pp. 1405–1422, Nov. 2019, doi: 10.1007/s10950-019-09876-5.

[14] S. Pasari and O. Dikshit, “Stochastic earthquake interevent time modeling from exponentiated Weibull distributions,” *Natural Hazards*, vol. 90, no. 2, pp. 823–842, Jan. 2018, doi: 10.1007/s11069-017-3074-1.

[15] V. F. Pisarenko, A. Sornette, D. Sornette, and M. V. Rodkin, “Characterization of the Tail of the Distribution of Earthquake Magnitudes by Combining the GEV and GPD Descriptions of Extreme Value Theory,” *Pure Appl. Geophys.*, vol. 171, no. 8, pp. 1599–1624, Aug. 2014, doi: 10.1007/s00024-014-0882-z.

[16] A. Dutfoy, “Earthquake Recurrence Model Based on the Generalized Pareto Distribution for Unequal Observation Periods and Imprecise Magnitudes,” *Pure Appl. Geophys.*, vol. 178, no. 5, pp. 1549–1561, May 2021, doi: 10.1007/s00024-021-02712-3.

[17] M. Zhang and H. Pan, “Application of generalized Pareto distribution for modeling aleatory variability of ground motion,” *Natural Hazards*, vol. 108, no. 3, pp. 2971–2989, Sep. 2021, doi: 10.1007/s11069-021-04809-3.

[18] M. Ren, “Uncertainty analysis of strong earthquake hazard estimation based on the generalized Pareto distribution model: a case study of the northeastern Tibetan Plateau,” *Annals of Geophysics*, vol. 64, no. 6, p. SE656, May 2022, doi: 10.4401/ag-8610.

[19] R. Chattamvelli and R. Shanmugam, *Continuous Distributions in Engineering and the Applied Sciences - Part I*. Cham: Springer International Publishing, 2021. doi: 10.1007/978-3-031-02430-6.

[20] C. Chaudhary and M. L. Sharma, “Probabilistic Models For Earthquakes With Large Return Periods In Himalaya Region,” *Pure Appl. Geophys.*, vol. 174, no. 12, pp. 4313–4327, Dec. 2017, doi: 10.1007/s00024-017-1667-y.

[21] Y. D. W. Sari and Sutikno, “Estimasi Parameter Generalized Pareto Distribution Pada Kasus Identifikasi Perubahan Iklim di Sentra Produksi Padi Jawa Timur,” *Jurnal Sains dan Seni ITS*, vol. 2, no. 2, pp. 2337–3520, 2013.

[22] A. A. Balkema and L. de Haan, “Residual Life Time at Great Age,” *The Annals of Probability*, vol. 2, no. 5, Oct. 1974, doi: 10.1214/aop/1176996548.

[23] J. Pickands, "Statistical Inference Using Extreme Order Statistics," *The Annals of Statistics*, vol. 3, no. 1, Jan. 1975, doi: 10.1214/aos/1176343003.
[24] S. Kotz and S. Nadarajah, *Extreme Value Distributions*. Imperial College Press, 2000. doi: 10.1142/p191.
[25] S. Ghosh and S. Resnick, "A discussion on mean excess plots," *Stoch. Process. Their Appl.*, vol. 120, no. 8, pp. 1492–1517, Aug. 2010, doi: 10.1016/j.spa.2010.04.002.
[26] S. Coles, *An Introduction to Statistical Modeling of Extreme Values*. London: Springer London, 2001. doi: 10.1007/978-1-4471-3675-0.
[27] C. Scarrott and A. Macdonald, "A Review of Extreme Value Threshold Estimation and Uncertainty Quantification," 2012.
[28] J. I. McCool, *Using the Weibull Distribution*. Wiley, 2012. doi: 10.1002/9781118351994.
[29] J. R. M. Hosking and J. R. Wallis, "Parameter and Quantile Estimation for the Generalized Pareto Distribution," *Technometrics*, vol. 29, no. 3, p. 339, Aug. 1987, doi: 10.2307/1269343.